2D/3D spin crossover porous coordination polymers based on isomeric tetrapyridyl benzene ligands

Wei-Wei Wu, Ze-Yu Ruan, Chen-Guang Shi, Jin-Tao Mai, Wen Cui, Zhao-Ping Ni*, Si-Guo Wu*, Ming-Liang Tong

Table S1. Crystallographic data and structural refinements for **1·2H$_2$O**.

Temperature	80 K	250 K
Formula	$C_{28}H_{28}B_2FeN_6O_2$	
Formula weight	558.03	
Crystal system	orthorhombic	
Space group	*F*222	
a / Å	10.7010(7)	11.012(4)
b / Å	15.5677(9)	15.769(5)
c / Å	18.8482(9)	18.997(6)
α / °	90	90
β / °	90	90
γ / °	90	90
V / Å^3	3139.9(3)	3298.7(19)
Z	4	4
$\rho_{calcd.}$ / g/cm^{-3}	1.180	1.124
μ / mm^{-1}	0.513	0.488
*F*000	1160.0	1160.0
Reflections collected	10371	10327
Independent reflections	1971 [R_{int} = 0.0378, R_{sigma} = 0.0319]	2001 [R_{int} = 0.0292, R_{sigma} = 0.0242]
GOF on F^2	1.080	1.066
R_1 [I ≥ 2σ(I)]a	R_1 = 0.0469	R_1 = 0.0377
wR_2 (all data)	wR_2 = 0.1216	wR_2 = 0.1061
Hooft parameter	0.31(3)	0.32(3)
CCDC No.	2144030	2144031

$^aR_1 = \sum||F_o| - |F_c||/\sum|F_o|$, $wR_2 = [\sum w(F_o^2 - F_c^2)^2/\sum w(F_o^2)^2]^{1/2}$.

Table S1. Crystallographic data and structural refinements for **2·2-NapSMe**.

Temperature	120 K	298 K
Formula	$C_{39}H_{34}B_2FeN_6S$	
Formula weight	696.25	
Crystal system	orthorhombic	
Space group	*Cmmm*	
a / Å	12.0275(9)	12.4250(3)
b / Å	15.8838(11)	16.2282(4)
c / Å	9.5912(6)	9.68021(19)
α / °	90	90
β / °	90	90
γ / °	90	90
V / Å^3	1832.3(2)	1951.87(7)
Z	2	2
$\rho_{calcd.}$ / g/cm^{-3}	1.262	1.185
μ / mm^{-1}	4.106	3.855
F000	724.0	724.0
Reflections collected	2274	3716
Independent reflections	1030 [R_{int} = 0.0289, R_{sigma} = 0.0321]	1117 [R_{int} = 0.0211, R_{sigma} = 0.0162]
GOF on F^2	1.135	1.235
R_1 [$I \geq 2\sigma(I)$][a]	R_1 = 0.0562	R_1 = 0.0580
wR_2 (all data)	wR_2 = 0.1653	wR_2 = 0.1726
CCDC No.	2144029	2144032

[a] $R_1 = \sum||F_o| - |F_c||/\sum|F_o|$, $wR_2 = [\sum w(F_o^2 - F_c^2)^2/\sum w(F_o^2)^2]^{1/2}$.

Table S3 Selected bond lengthes of **1·2H$_2$O**.

Temperature / K	80 K	250 K
Fe1–N1[a] / Å	2.038(4)	2.124(3)
Fe1–N1 / Å	2.038(4)	2.124(3)
Fe1–N2[b] / Å	2.130(3)	2.233(2)
Fe1–N2[a] / Å	2.130(3)	2.233(2)
Fe1–N2 / Å	2.130(3)	2.233(2)
Fe1–N2[c] / Å	2.130(3)	2.233(2)
$\langle$Fe–N$\rangle_{av}$ / Å[d]	2.099	2.197
N1–C1 / Å	1.153(6)	1.132(5)
C1–B1 / Å	1.564(8)	1.599(13)

[a]-X,1-Y,+Z ; [b]+X,1-Y,-Z ; [c]-X,+Y,-Z ; [d]average Fe−N bond length; [f]Octahedral distortion parameters.

Table S4 Selected bond angles of **1·2H$_2$O**.

Temperature / K	80 K	250 K
∠N1^a–Fe1–N1 / °	180	180.0
∠N1^a–Fe1–N2^b / °	93.16(12)	93.48(9)
∠N1^a–Fe1–N2^a / °	93.16(12)	93.48(9)
∠N1–Fe1–N2^a / °	86.84(12)	86.52(9)
∠N1^a–Fe1–N2^c / °	86.84(12)	86.52(9)
∠N1–Fe1–N2^b / °	86.84(12)	86.52(9)
∠N1–Fe1–N2 / °	93.16(12)	93.48(9)
∠N1–Fe1–N2^c / °	93.16(12)	93.48(9)
∠N1^a–Fe1–N2 / °	86.84(12)	86.52(9)
∠N2^c–Fe1–N2^a / °	89.33(14)	88.46(12)
∠N2^a–Fe1–N2 / °	91.02(14)	91.96(12)
∠N2^c–Fe1–N2 / °	173.7(2)	173.04(17)
∠N2^b–Fe1–N2 / °	89.33(14)	88.46(12)
∠N2^c–Fe1–N2^b / °	91.02(14)	91.96(12)
∠N2^b–Fe1–N^a / °	173.7(2)	173.04(17)
∠C1–N1–Fe1 / °	180.0	180.0
∠C6–N2–Fe1 / °	121.6(3)	122.4(2)
∠N2–C6–C5 / °	122.2(4)	123.4(3)
∠C4–C3–C2 / °	117.2(4)	117.1(2)
∠C4–C3–C7 / °	122.7(4)	122.7(3)
∠N2–C2–C3 / °	124.4(3)	124.5(2)
∠C7^d–C7–C8 / °	119.3(2)	119.37(16)
∠C8–C7–C3 / °	118.2(3)	118.2(2)
∑Fe^e / °	28.66	34.84

^{a}-X, 1-Y, +Z ; ^{b}+X,1-Y,-Z ; ^{c}-X,+Y,-Z ; ^{d}1/2-X,+Y,1/2-Z; ^{e}Octahedral distortion parameters.

Table S5 Selected bond lengthes of **2·2-NapSMe**.

Temperature / K	120 K	298 K
Fe1–N2[a] / Å	2.002(3)	2.197(3)
Fe1–N2 / Å	2.002(3)	2.197(3)
Fe1–N2[b] / Å	2.002(3)	2.197(3)
Fe1–N2[c] / Å	2.002(3)	2.197(3)
Fe1–N1[a] / Å	1.946(4)	2.141(5)
Fe1–N1 / Å	1.946(4)	2.141(5)
$\langle Fe–N \rangle_{av}$ / Å[f]	1.983	2.178
N2–C6 / Å	1.380(5)	1.394(5)
N2–C2 / Å	1.326(5)	1.292(5)
N1–C1 / Å	1.134(8)	1.131(9)
C8–C7 / Å	1.398(4)	1.389(4)
C8–C7[d] / Å	1.398(4)	1.389(4)
C4–C7 / Å	1.480(5)	1.485(4)
C4–C5 / Å	1.439(5)	1.429(5)
C4–C3 / Å	1.358(5)	1.346(6)
C7–C7[e] / Å	1.409(6)	1.409(6)
C1–B1 / Å	1.616(13)	1.658(18)
C6–C5 / Å	1.382(7)	1.383(7)
C3–C2 / Å	1.378(7)	1.380(7)

[a]2-X,1-Y,2-Z ; [b]2-X,1-Y,+Z ; [c]+X,+Y,2-Z ; [d]1-X,1-Y,+Z ; [e]+X,+Y,1-Z ; [f]average Fe–N bond length.

Table S6 Selected bond angles of **2·2-NapSMe**.

Temperature / K	120 K	298 K
∠N2[a]–Fe1–N2[b] / °	91.03(16)	91.34(15)
∠N2[c]–Fe1–N2 / °	91.03(16)	91.34(15)
∠N2[a]–Fe1–N2 / °	180	180.0
∠N2[b]–Fe1–N2[c] / °	180	180.0
∠N2[a]–Fe1–N2[c] / °	88.97(16)	88.66(15)
∠N2[b]–Fe1–N2 / °	88.97(16)	88.66(15)
∠N1[a]–Fe1–N2[a] / °	90.000(1)	90.000(1)
∠N1–Fe1–N2[c] / °	90	90.0
∠N1–Fe1–N2[b] / °	90.000(1)	90.000(1)
∠N1[a]–Fe1–N2 / °	90	90.0
∠N1–Fe1–N2 / °	90.000(1)	90.000(1)
∠N1[a]–Fe1–N2[c] / °	90.000(1)	90.000(1)
∠N1[a]–Fe1–N2[b] / °	90	90.0
∠N1–Fe1–N2[a] / °	90	90.0
∠N1–Fe1–N1[a] / °	180	180.0
∠C6–N2–Fe1 / °	118.0(2)	117.0(2)
∠C2–N2–Fe1 / °	125.5(3)	127.0(3)
∠C2–N2–C6 / °	116.4(4)	116.0(4)
∠C1–N1–Fe1 / °	180.0	180.0
∠C7–C8–C7[d] / °	124.0(4)	123.4(4)
∠C3–C4–C7 / °	126.2(3)	125.7(3)
∠C8–C7–C4 / °	117.0(3)	117.3(3)
∠N1–C1–B1 / °	180.0	180.0
∠C5–C6–N2 / °	122.5(4)	121.9(4)
∠C6–C5–C4 / °	119.0(4)	119.0(4)
∠C4–C3–C2 / °	120.7(4)	120.6(4)
∠N2–C2–C3 / °	124.3(4)	125.2(4)
∑Fe[f] / °	4.12	5.36

[a]2-X,1-Y,2-Z; [b]2-X,1-Y,+Z ; [c]+X,+Y,2-Z ; [d]1-X,1-Y,+Z ; [e]+X,+Y,1-Z; [f]Octahedral distortion parameters.

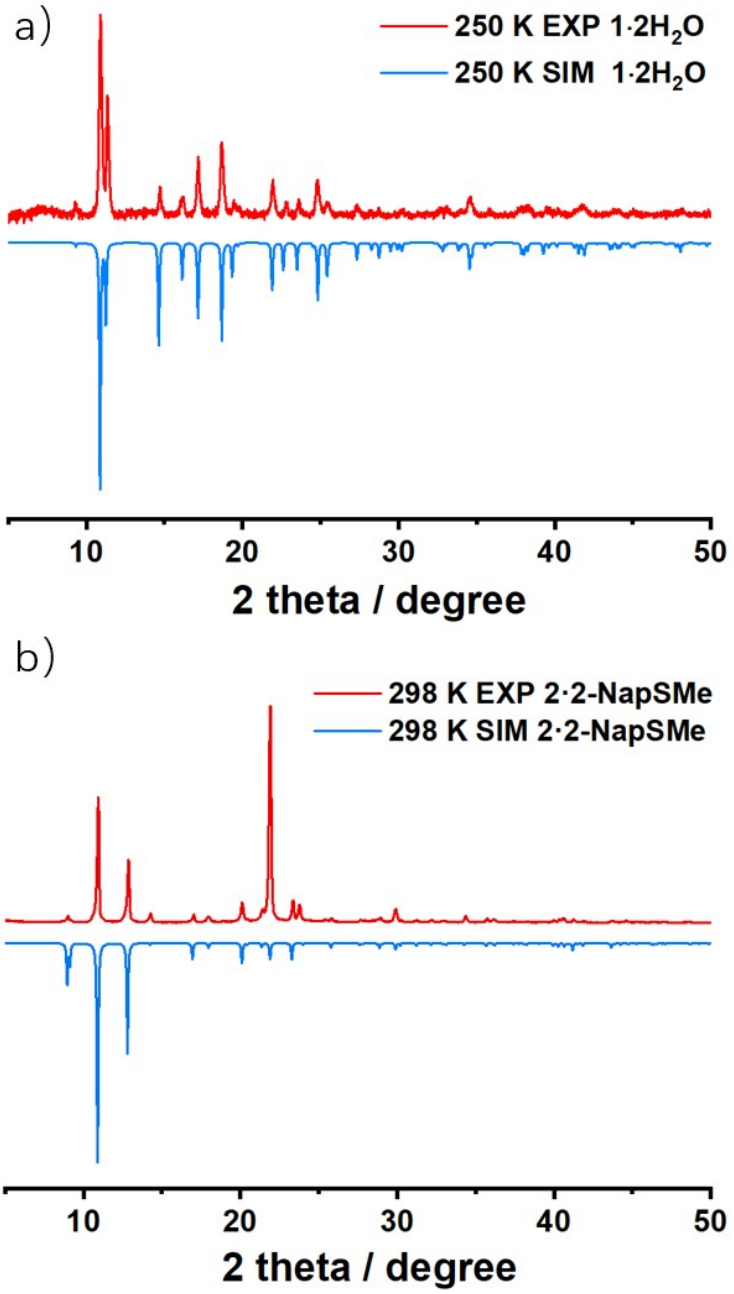

Figure S1. The experimental and simulated powder X-ray diffraction (PXRD) patterns for **1·2H$_2$O** (a); the experimental and simulated powder PXRD patterns for **2·2-NapSMe** (b).

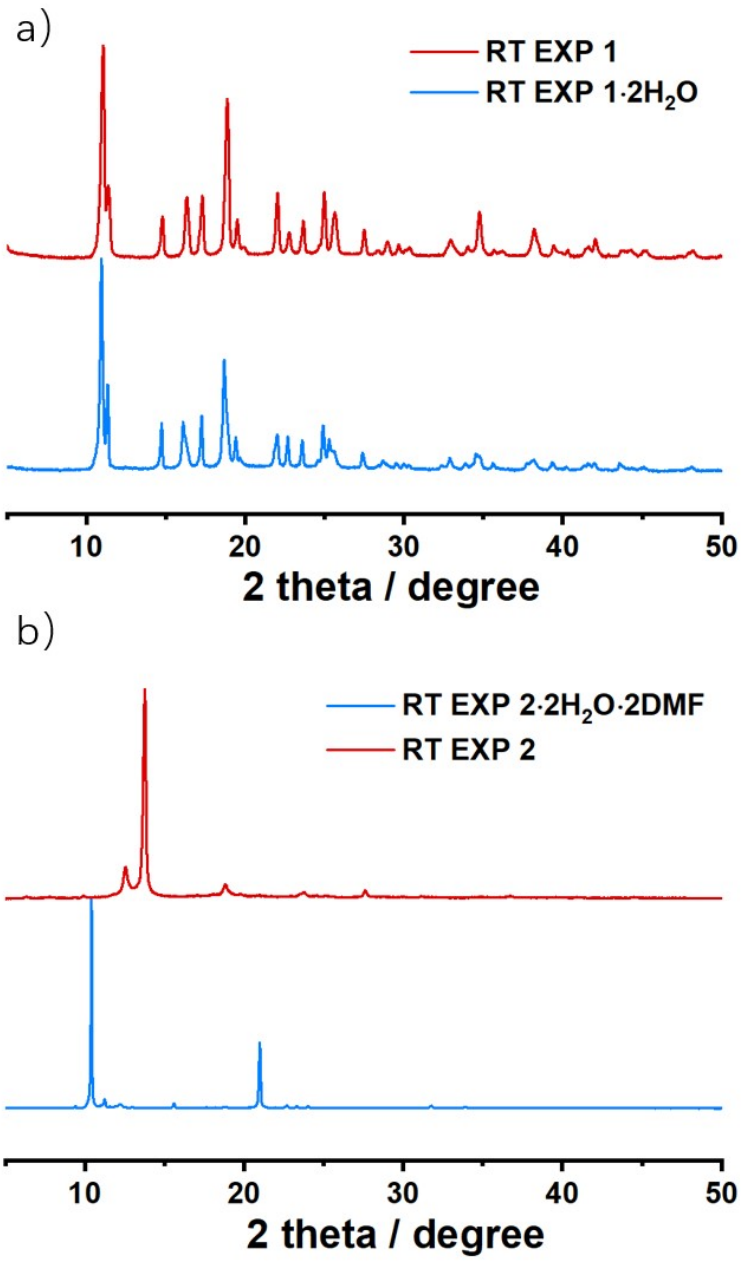

Figure S2. The experimental powder X-ray diffraction (PXRD) patterns for a) **1** and **1·2H$_2$O**; b) **2** and **2·H$_2$O·3DMF**.

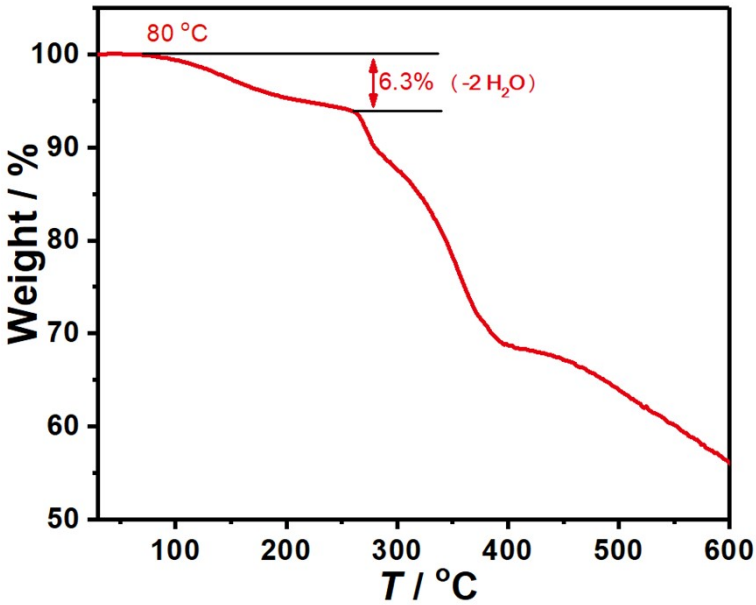

Figure S3. Thermogravimetric analysis (TGA) curve of **1·2H$_2$O** at a heating rate of 10 K min^{-1}.

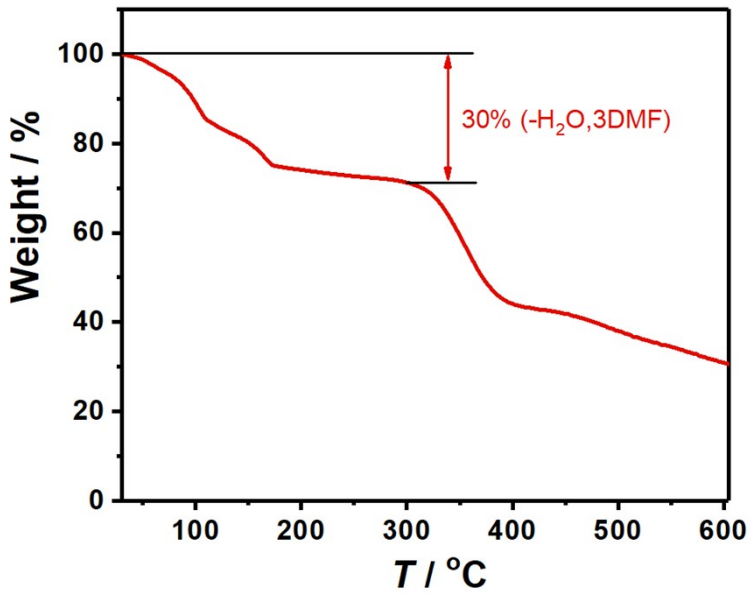

Figure S4. Thermogravimetric analysis (TGA) curve of **2·H$_2$O·3DMF** at a heating rate of 10 K min^{-1}.

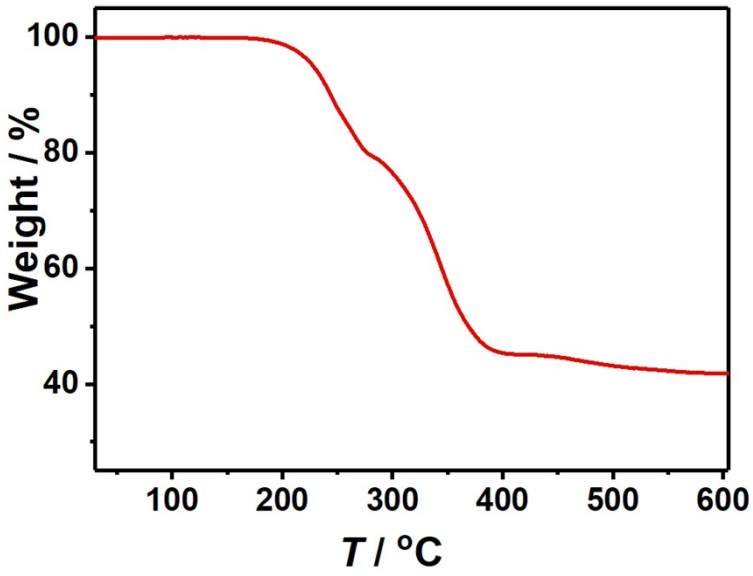

Figure S5. Thermogravimetric analysis (TGA) curve of **2·2-NapSMe** at a heating rate of 10 K min^{-1}.

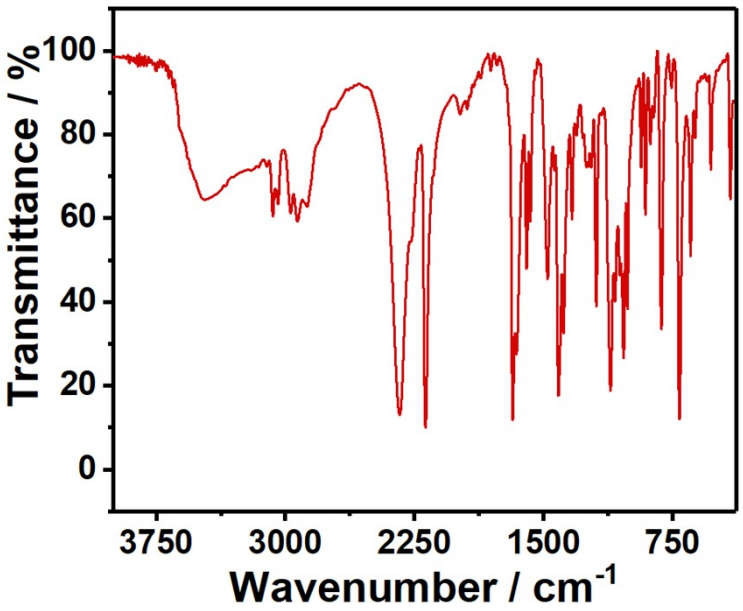

Figure S6. The infrared (IR) spectrum of **1·2H$_2$O**.

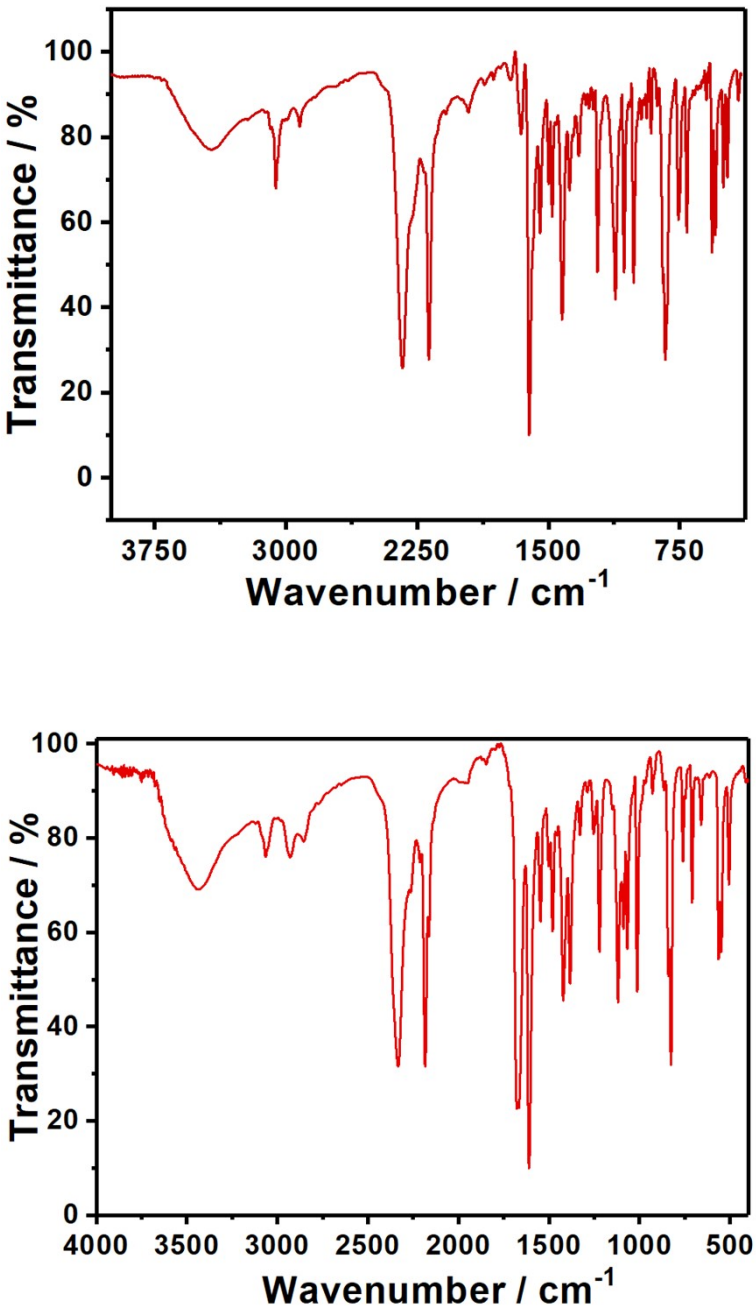

Figure S7. The infrared (IR) spectrum of **2·2-NapSMe** (up) and **2·H_2O·3DMF** (down).

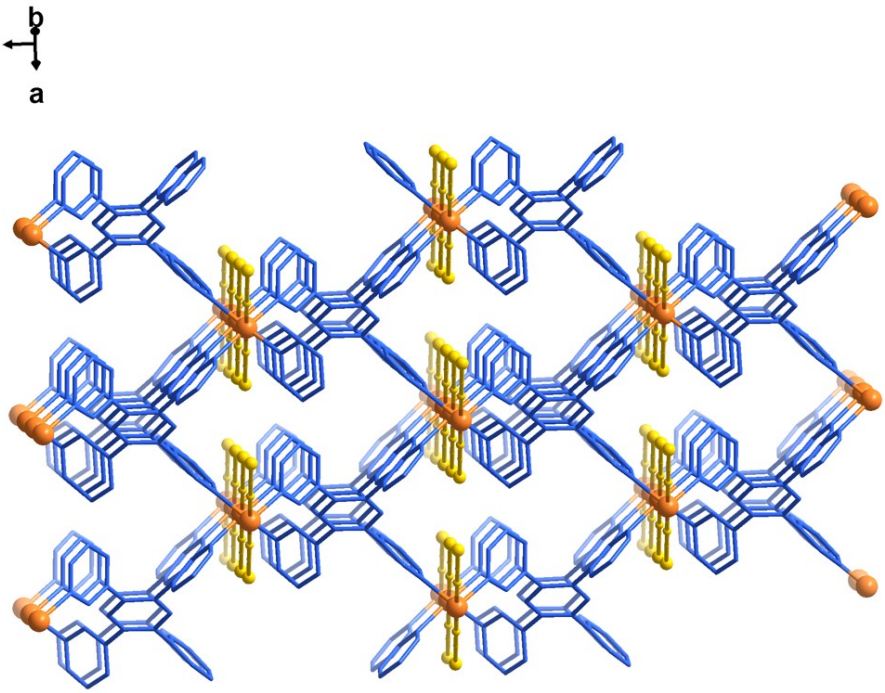

Figure S8. The 3D framework of **1**, color code: Fe^{II}, orange; $NCBH_3^-$, golden; 3-tpb, blue.

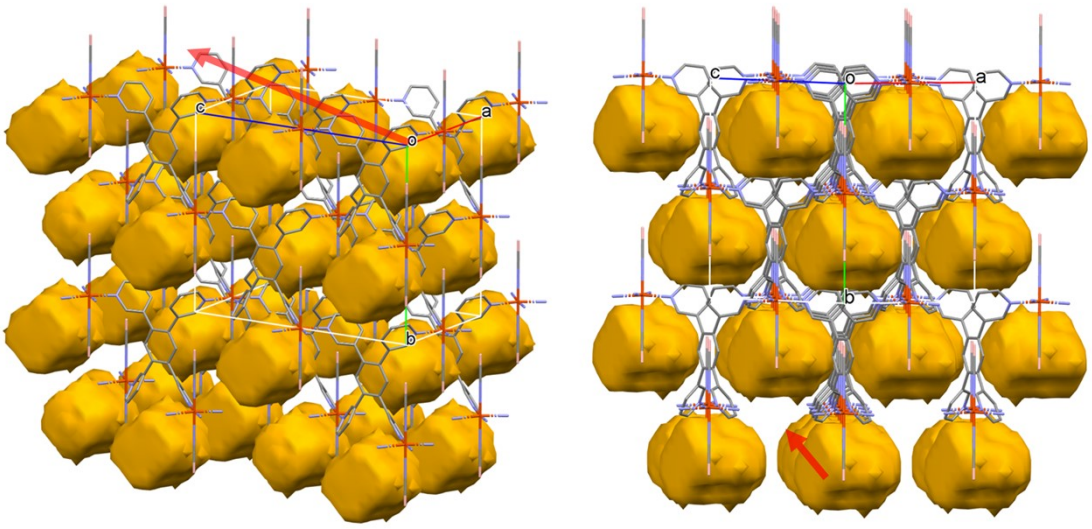

Figure S9. The 3D framework of **1·2H$_2$O** with the cavities.

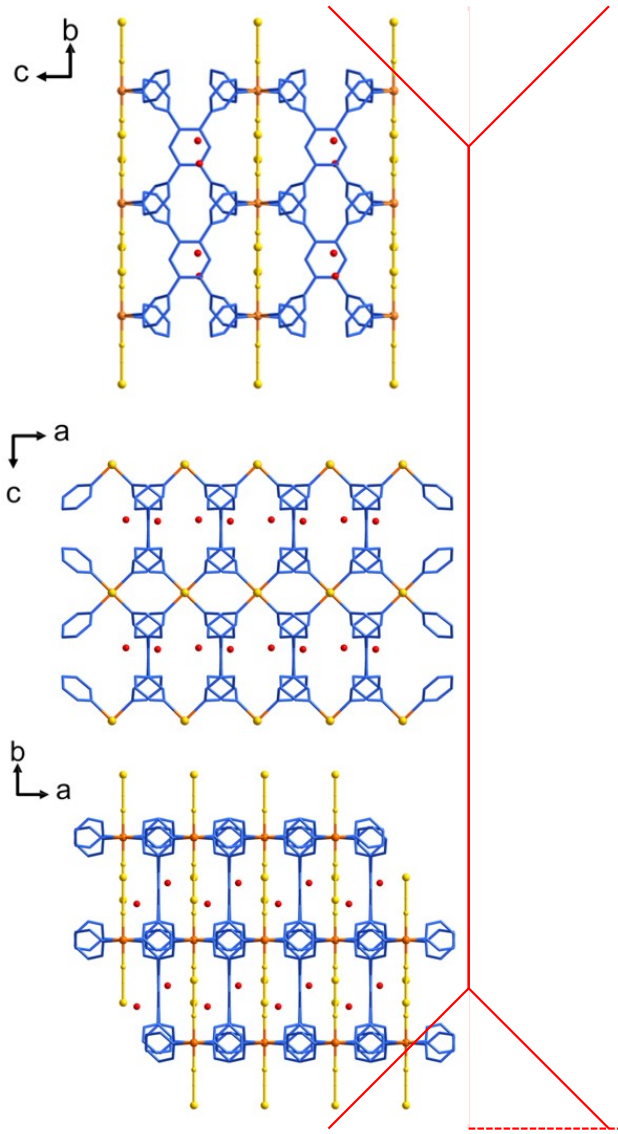

Figure S10. Packing view of **1·2H$_2$O** along the *a, b, c* axis. Color code: Fe^{II}, orange; 3-tpb, blue; NCBH$_3^-$, golden; O, red. Partial hydrogen atoms are omitted for clarity.

Comment [□□□]: 删掉了水的氢原子

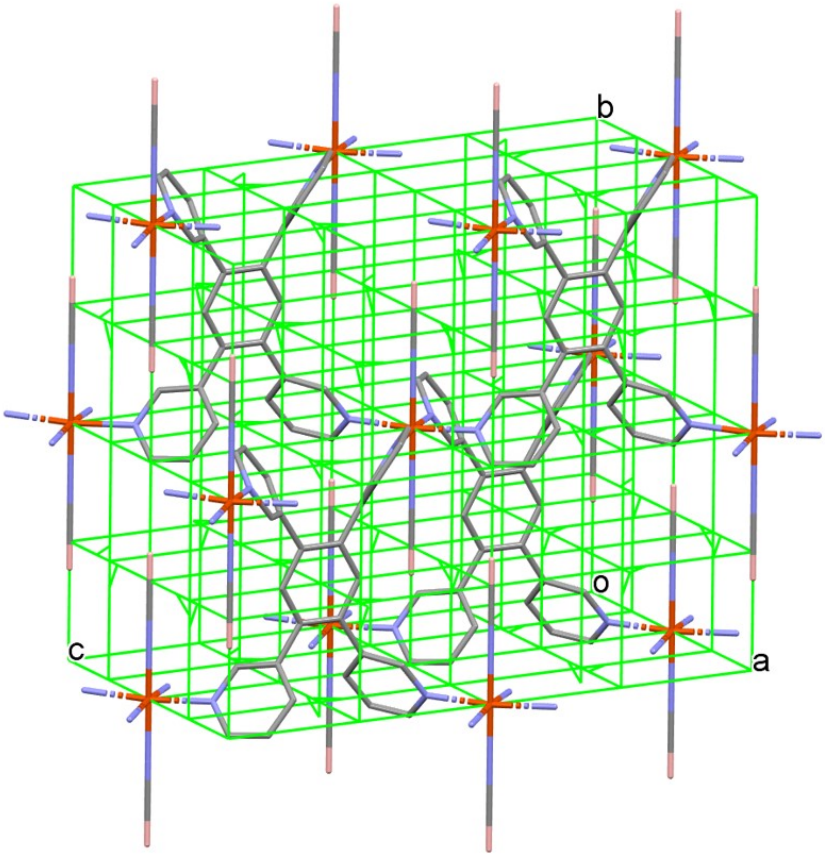

Figure S11. The 3D framework of **1** with symmertry elements (2-fold axis, green line).

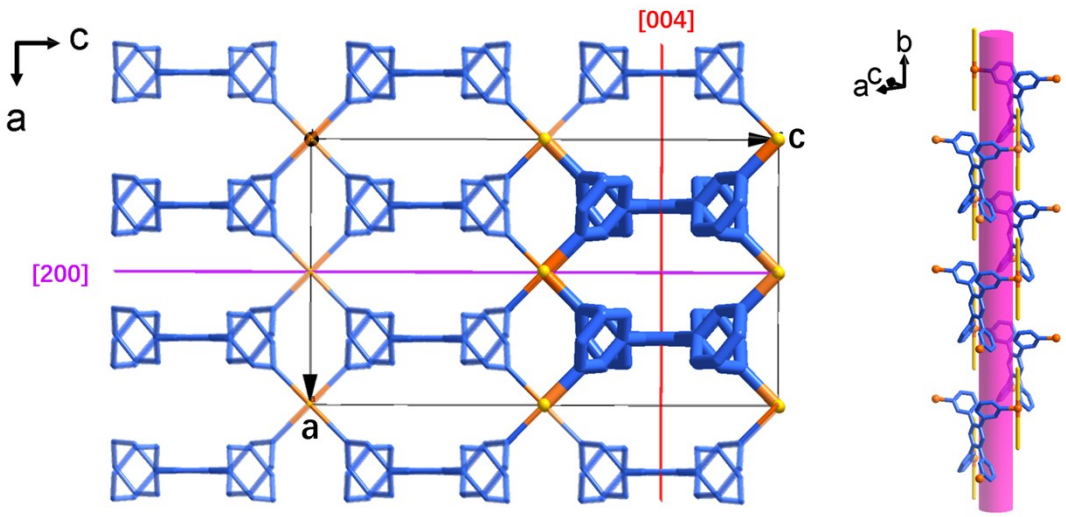

Figure S12. The 2_1 helical chains viewed from the *b*-axis of **1**.

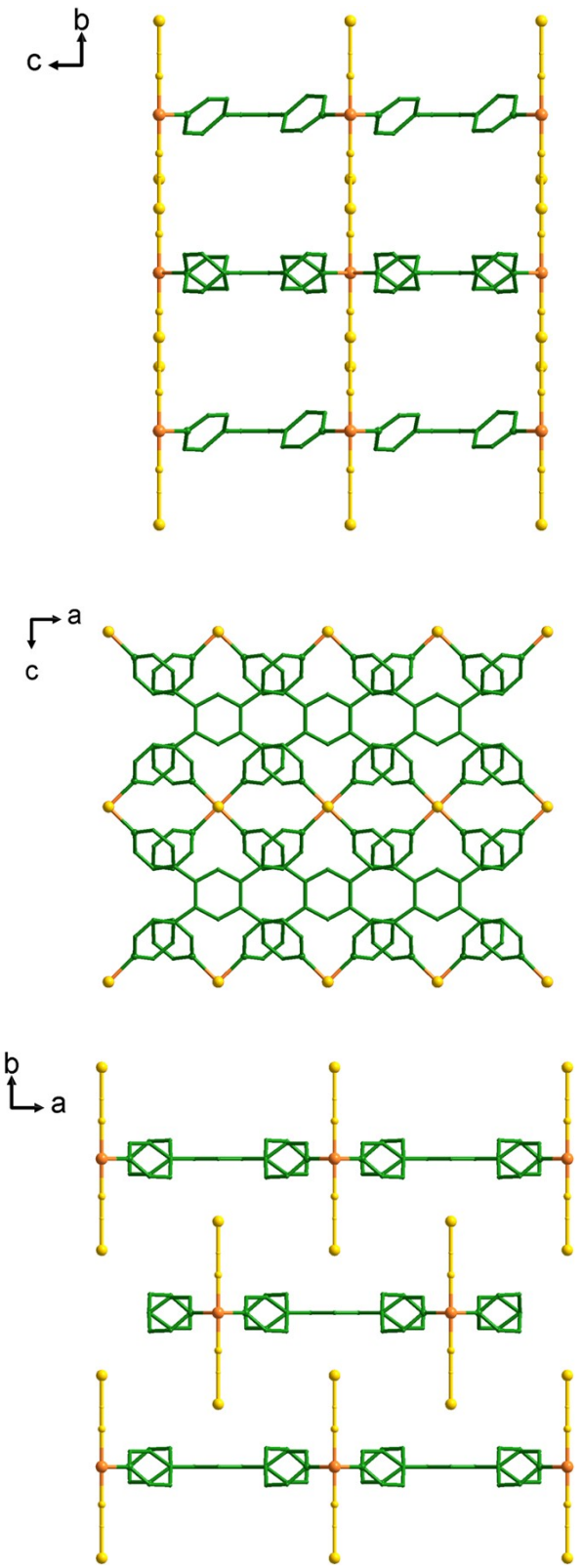

Figure S13. Packing view of **2** along the *a, b, c* axis. Color code: Fe^{II}, orange; 4-tpb, green; $NCBH_3^-$, golden. Hydrogen atoms and guests are omitted for clarity.

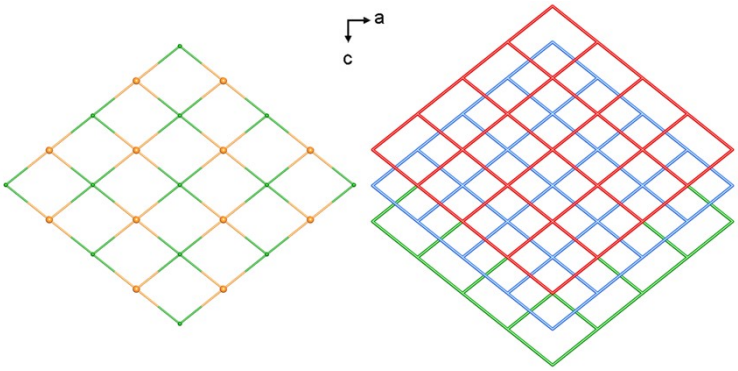

Figure S14. The 3D framework of **2** with the square lattice net topology. Color code: Fe^{II}, orange; 4-tpb, green (left); different colors represent different layers (right).

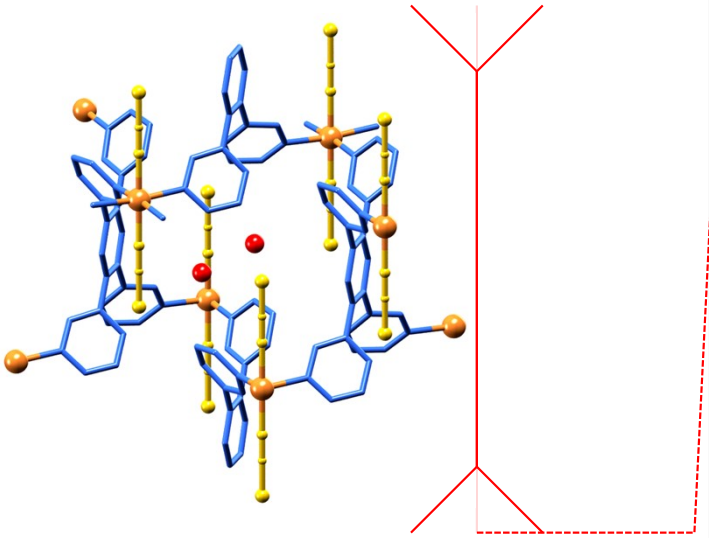

Figure S15. Structural representation of **1·2H$_2$O**, Color code: Fe^{II}, orange; $NCBH_3^-$, golden; O, red; 3-tpb, blue.

Comment [□□□]: 删除了含硫客体的那个

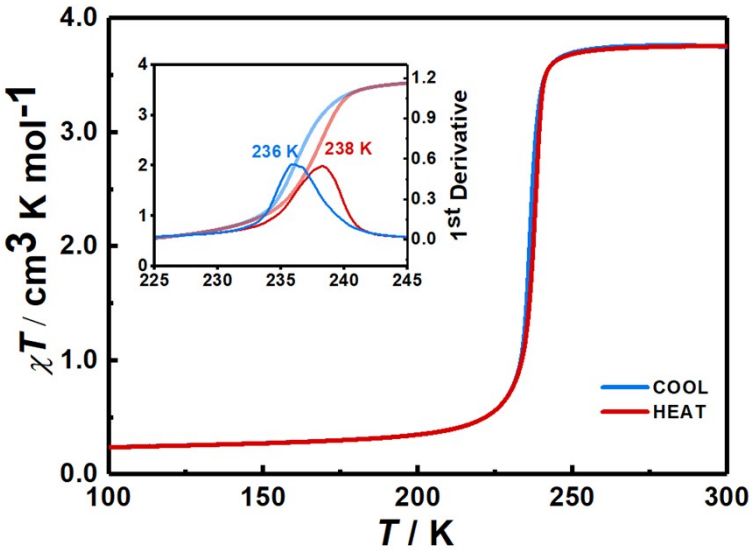

Figure S16. The temperature-dependent magnetic susceptibility data of **2·2-NapSMe** Inset: the expanded view of thermal hysteresis loop and the corresponding 1st derivative curves.

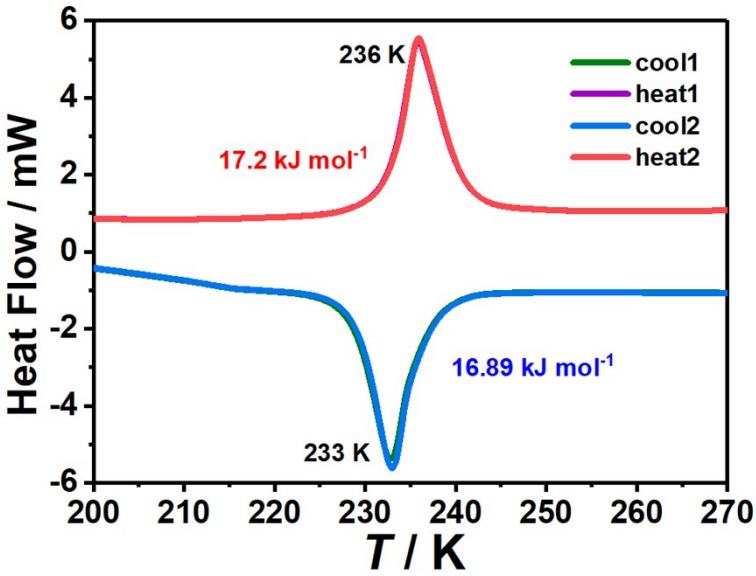

Figure S17. Differential scanning calorimetry (DSC) curves with a sweep rate of 10 K min^{-1} for **2·2-NapSMe**.

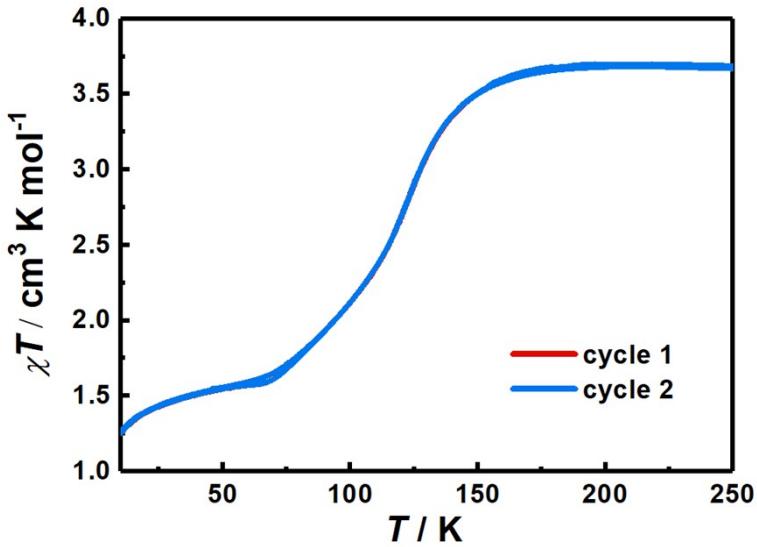

Figure S18. The temperature-dependent magnetic susceptibility data of **1·2H$_2$O** with a sweep rate of 2 K min^{-1}.

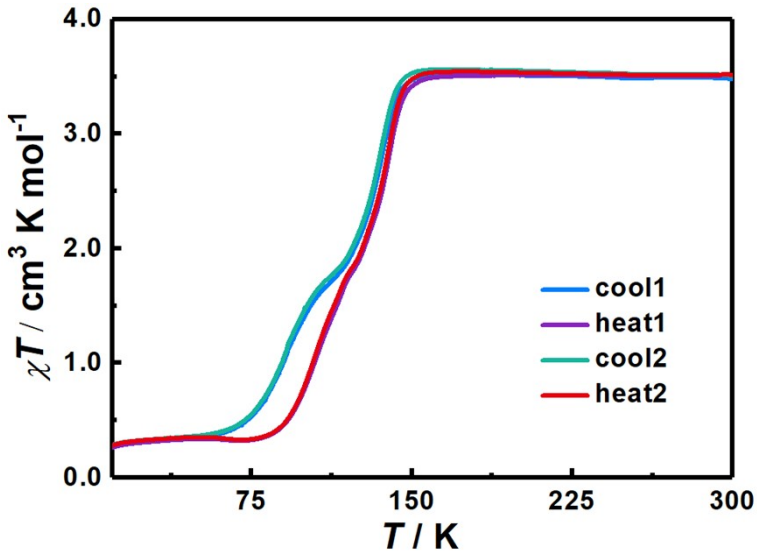

Figure S19. The temperature-dependent magnetic susceptibility data of **2·H$_2$O·3DMF** with a sweep rate of 2 K min^{-1}.

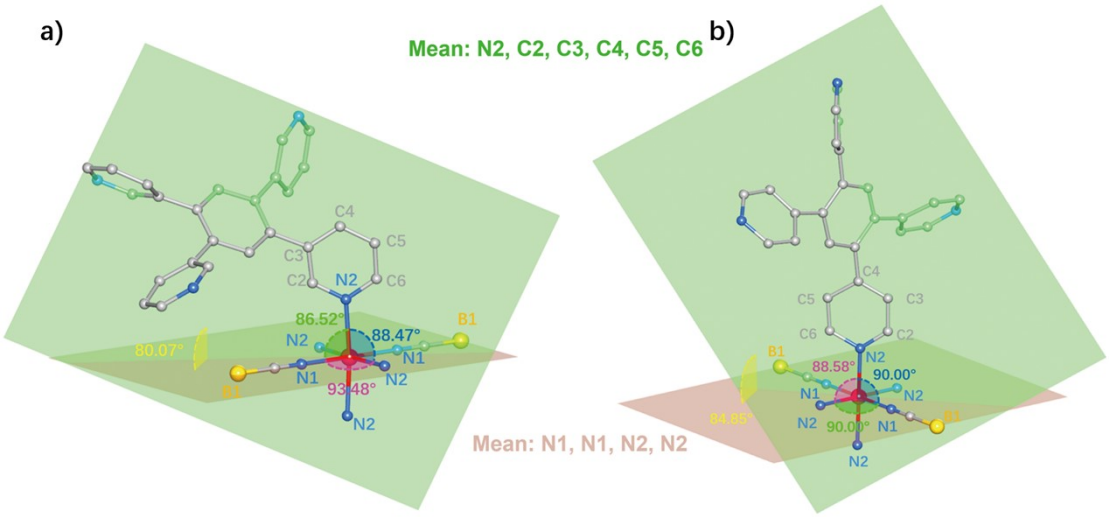

Figure S20. Structural analyses for a) **1·2H$_2$O** (250 K) and b) **2·2-NapSMe** (298 K). Colour code: Fe^{II}, magenta; B, golden; N, blue; C, grey. The hydrogen atoms and disordered moieties in 4-tpb are omitted for clarity. The green/tawny planes are designated by pyridyl moiety and coordinated atoms of N2 and N1.